Channeling flux in single crystals with interstitial atoms: Impurity concentration dependence*

G. Della Mea, A. V. Drigo, S. Lo Russo, P. Mazzoldi, and S. Yamaguchi†
Istituto di Fisica dell'Università, Unità del Gruppo Nazionale di Struttura della Materia, Padova, Italy

G. G. Bentini, A. Desalvo‡, and R. Rosa
Laboratorio per la Chimica e Tecnologia dei Materiali e Componenti per l'Elettronica, Consiglio Nazionale delle Ricerche, Bologna, Italy

(Received 25 February 1974)

The dependence upon interstitial impurity concentration of the flux of channeled particles has been determined both experimentally and by computer simulations. Experiments were carried out on TiO_x, with x ranging from 0.11 to 0.39, and computer simulations on SiB_x, with x ranging from 0.1 to 0.5. The similarity between the two systems was checked by computer, with particular reference to the relative strength of the interstitial and lattice-atom arrays. Both experiments and calculations show that the interstitial string is much more effective than the plane; in fact, channeling effects due to the former are clearly displayed for $x = 0.2$, while the latter does not produce any channeling effect up to $x = 0.5$. The computer calculations show that these results can be understood in terms of the relative effect of the host-lattice and interstitial-array potentials. Both experiments and calculations show that at an intermediate incidence angle between axial and planar orientations the beam can distinguish between stronger and weaker strings and penetrates with preference near the latter ones, giving rise to a much higher yield at the interstitial site.

I. INTRODUCTION

A well known application of ion channeling is the location of impurity atoms in crystal lattices, e.g., in implanted materials. The determination of the flux distribution of the particles of the analyzing beam inside axial and planar channels is essential in the interpretation of these experiments. To this purpose it is necessary to simulate the flux inside the crystal either by a Monte Carlo[1-3] or an analytical[4,5] model and compare the yield of some particular process (e.g., nuclear reaction, Rutherford backscattering) with the computed flux (of course both must be normalized to the random value). At low impurity concentrations, the flux distribution is solely determined by the atoms of the host lattice. The complex situation arising in this case has been analyzed in detail very recently by comparing computer simulations for different locations of Br atoms in Fe with the experimental angular distribution of backscattering yield.[6]

However, as the concentration increases, strings and planes of impurity atoms are built which will likewise affect the flux distribution. This is clear when the impurity concentration is so high that a compound with a new crystal lattice characterized by strings and planes built with different atoms, i.e., of different steering power, is formed. However, the experiments showed that also in this extreme case things are not so simple, in particular, when the difference between the atomic numbers of the two species is sufficiently high. It was observed that, while strings built only by the low-Z element are always effective, the planes of the light species may give rise to quite different effects. In some compounds these planes are very weak [e.g., in $BaTiO_3$ (Ref. 7) and in SiO_2 (Ref. 8)], in others only the densest plane produces channeling effects [e.g., in CaF_2 and BaF_2 (Ref. 9)], while in some others all these planes are completely absent [e.g., in UO_2 (Ref. 10)].

For these reasons we decided to analyze experimentally a system in which the concentration of light atoms could be varied in a wide enough range. Our experimental results on the TiO_x system[11] showed how the steering power of impurity strings and planes varies with increasing concentration. It was possible to follow the transition from the most common low-concentration regime, in which the effect of the host lattice on the flux distribution prevails, to the situation in which the impurity concentration is high enough to give rise to channeling effects. In particular, our experiments confirmed that the impurity string produces steering effects on the particle beam at a much lower concentration than the impurity plane. Therefore it is necessary to be very careful in drawing conclusions on the location of impurity atoms in a range of concentrations in which the impurity string is already able to produce channeling effects while the planes are still too weak.

A simple analysis in terms of continuum theory and fundamentally based on summing the contribution due to the interaction with one string (or plane) at a time[7,10] gave good agreement for $\psi_{1/2}$ and χ_{min} values in the planar but not in the axial case. A

preliminary computer simulation was tried using an available program for the SiB_x system, obtaining a qualitative agreement with the experimental results as a function of concentration.[11] The choice of SiB_x was justified because some elements of the crystal symmetry and the ratio of atomic numbers are comparable to the TiO_x system.

As a consequence, a more accurate theoretical analysis was needed. In the present paper we extend to the whole channel area the calculation of the flux distribution in the SiB_x system for different boron concentrations and crystal orientations and compare this distribution with the corresponding continuum potential, both for the axial and planar cases. In order to support the feasibility of a comparison with the experimental results on the TiO_x system, we compared the potential distribution at various concentrations in the two systems. On the basis of these calculations it has been possible to give a satisfactory explanation of the most typical and significant experimental results.

II. COMPUTER RESULTS

A. SiB_x system

The computer model is the same as described in detail in a series of previous papers.[12] The model uses the standard Lindhard atomic potential and takes into account the dependence of energy loss from impact parameter, thermal vibrations, electron scattering, multiple scattering in a thin surface oxide film (30 Å), and angular divergence of the incident beam (0.03°). The most important change is the memorization of the flux of ions going through a given channel section. This was calculated in the usual way[1] by dividing the channel area into grid squares of appropriate size (0.039 $Å^2$, which corresponds to $\sim a_{TF}^2$ and is equal to 3.75×10^{-3} times the channel area) and recording the number of ions going through each of them. In order to save computer time the number of analyzed ion paths was limited to 100–200. As a consequence, to improve statistics, we averaged over a thickness of 600 Å, which in our case ($\langle 100\rangle$ axis in silicon) corresponds to ~150 atomic spacings. Moreover, we summed over the four equivalent squares which occur due to the symmetry of the crystal axis: This is legitimate both for parallel incidence to the $\langle 110\rangle$ axis and tilted incidence along the $\{110\}$ plane. The flux was normalized to the random value.

Figure 1 shows the projection of the silicon crystal lattice both perpendicular and parallel to the [110] axis. The interstitial site is denoted by an open circle and the lattice site by a full one. Positions on different (110) planes are specified by the numbers 1 and 2 on the left side of the figure and are clearly displayed on the right side. Computations were made for two different locations of the interstitial boron atom, that is, corresponding to the location of oxygen in the TiO_x system. In the first case the interstitial was considered at the center of the [110] axial channel (see left side of Fig. 1): The incidence angle with the axis was varied by tilting along the $(1\bar{1}0)$ mixed plane shown in the figure. In the second case, shown in the right side of Fig. 1, the interstitial was halfway along one of the four long sides of the pseudohexagon which bounds the $[1\bar{1}0]$ axial channel perpendicular to the former. Notice that the interstitial is projected on the side, since in our model all six lattice atoms of the pseudohexagonal channel are considered to be lying on the same plane. This location was chosen to simulate the flux across the (110) plane: In this case the tilting angle is still along this plane, but now we have pure boron sheets at half the interplanar distance between pure silicon sheets. In both cases the interstitial was encountered after a fixed number of steps along the channel, chosen in such a way to give the desired composition.

For simplicity no elastic deformation of the host lattice was taken into account. Thermal vibrations of the interstitial were simulated by assuming a local larger Debye temperature associated with the lighter mass: The approximate shift was evaluated by assuming a Debye frequency equal to the frequency of the local mode calculated according to the procedures outlined in many standard textbooks (see, e.g., Ref. 13). The local stopping

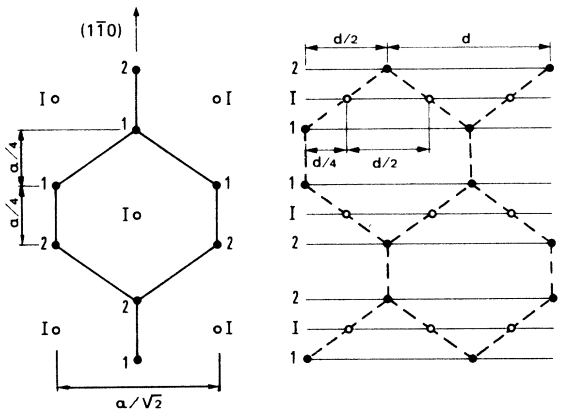

FIG. 1. Front and side view of the [110] channel in silicon; *a* denotes the lattice constant and *d* the spacing along the $\langle 110\rangle$ string. *I* denotes the interstitial string; 1 and 2 lattice strings whose atoms lie on two different (110) planes. Open circles denote interstitials and full circles lattice atoms. In the lateral view the perpendicular channel $[1\bar{1}0]$ is drawn to show the resulting interstitial position.

power near the interstitial was evaluated in the same way as for the lattice atoms, by simply changing the values of atomic number and Thomas-Fermi screening radius.

Calculations were performed for 1-MeV deuterons in order to compare with the experiments on TiO_x. The flux values used refer to a depth of 0.3 μm below the surface. The computation time was ~2 sec per ion, including the time to operate the plotter routines (see below). Computations were carried out on the CDC 6600 of the "Centro di Calcolo Elettronico Interuniversitario dell'Italia Nord-Orientale."

The computer output can be visualized in two ways, shown in Figs. 2 and 3, respectively. The former is the dot-density plot as given directly by an off-line Benson 111 plotter, while the latter is the flux-contour plot obtained from computed results. Owing to the statistical nature of the results the contours are somewhat qualitative but the main features are clearly evident. Therefore in the following only flux-contour plots will be shown. Both figures refer to the ⟨110⟩ axial incidence and to different concentrations of boron atoms, lying at the center of the channel (for simplicity only a quarter of the channel is shown). The sequence shows the progressive displacement of the maximum flux towards the center of the new channel. We see that already at the composition $x = 0.1$ the interstitial row is able to repel the ion flux to some extent, even though the nuclear encounter probability within a distance of $\sim 1.5 a_{TF}$ is still of the order of the random value. At $x = 0.5$ the symmetry of the new axial channel is completely built on, even though the strength of the Si and B strings is not the same.

Figure 4 shows the corresponding Lindhard continuous string potential. In order to avoid divergences at the string, the approximation for thermal vibrations due to Foti *et al.*[14] was used (in any case this correction is important only at distances of the order of the amplitude of vibration, ~0.1 Å). The close resemblance between Figs. 3 and 4 can easily be noticed. Other curves, not given here, show that at x values as low as 0.025, the interstitial string already produces a definite pattern, giving 1.7 eV for the potential at the row. However, for x values lower than 0.1 the effect of the interstitial string is much smaller than those of lattice atoms: Therefore the flux is still peaked not far from the center of the channel. An estimate of the relative effects of the two types of string on the basis of continuum theory will be given below.

A completely different situation occurs for

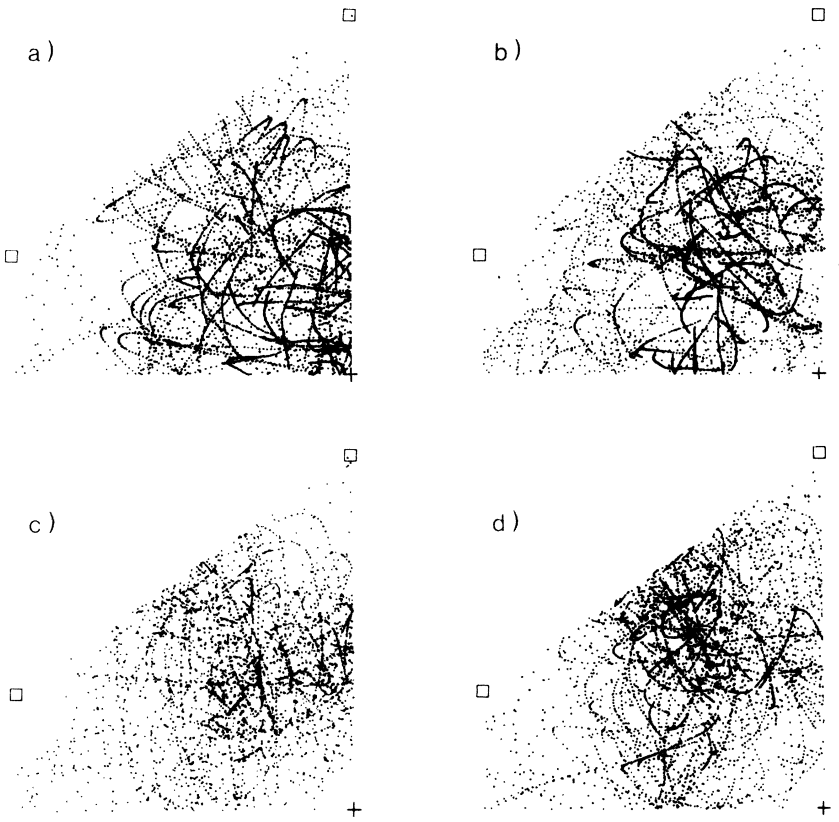

FIG. 2. Dot-density plot of 100 trajectories of 1-MeV deuterons incident parallel to the ⟨110⟩ axis in silicon containing boron atoms at the midchannel axis, for different compositions SiB_x. The paths are plotted from 2400 to 3000 Å below the surface; for clarity only one point each three steps of the ion path is plotted. □, Si site; +, B site (only one quarter of the channel is shown). (a) $x = 0$; (b) $x = 0.1$; (c) $x = 0.25$; (d) $x = 0.5$.

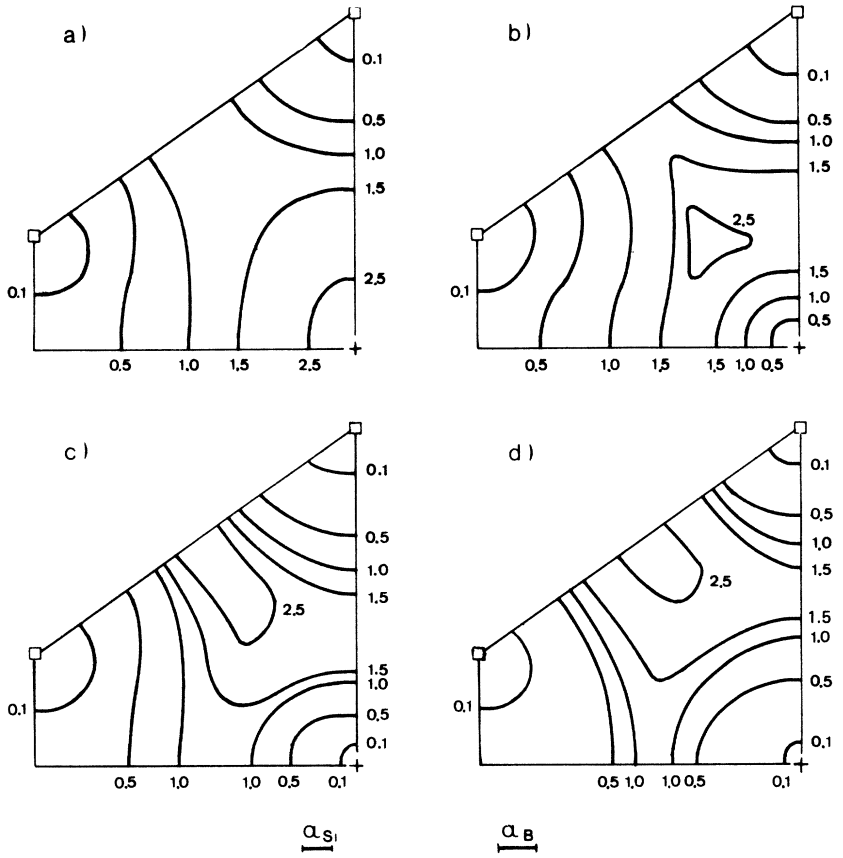

FIG. 3. Flux-contour plot for the same conditions as Fig. 2. a_{Si} and a_B, the Thomas-Fermi radii relative to the two atoms, are shown for comparison on the same scale.

atomic planes. Figure 5(a) shows the flux distribution normal to the {110} plane of pure silicon with increasing boron concentration at the midplane position (for simplicity only half the channel is drawn). Incidentally we notice that the structure of curve (a) ($x=0$) is similar to the one observed by Carstanjen and Sizmann.[3] With increasing impurity concentration the peak at midplane decreases: Only at a much higher concentration than in the axial case ($x=0.5$) does the effect of the boron plane begin to be displayed and the flux peak is pushed away from the midplane position. However, the flux at the interstitial plane drops below the random value only for still higher concentrations ($x=1$). This is confirmed by Lindhard's continuum potential shown in Fig. 5(b): Only at composition $x=1$ does the interstitial plane stand out distinctly. We notice that no temperature correction was made in this case, since it is less important and amounts to about 20% on the plane.[15]

A very simple estimate of the relative effect of strings or planes of interstitials and lattice atoms can be made as follows: First let us evaluate the average transverse energy of a particle under channeling conditions. The most important contribution at our low thicknesses is given by the potential energy at the starting point of the channeled trajectory. Table I shows the values of the average initial transverse energy evaluated from the continuum potentials previously shown, excluding the regions closer than the Thomas-Fermi screening radius to lattice strings (or planes), and the potential value at the interstitial string (or plane) with increasing composition x. Notice that the average initial transverse energy depends very slightly on concentration; i.e., it is mainly determined by the host-lattice strings (or planes).

The increase in transverse energy due to electron scattering turns out to be small compared to the initial transverse energy and can be neglected as a first approximation. To have an indication of the reliability of the transverse-energy data shown in Table I, we have compared them with Monte Carlo results. Let us take 7 and 2.5 eV as the average transverse-energy values for axis and plane, respectively. The corresponding average angles are found to be 2.6 and 1.6 mrad, in excellent agreement with the average angles between the emergence direction of the computed trajectories and the string and plane (2.45 and 1.4 mrad, respectively). The agreement between the results of continuum theory and Monte Carlo simulations

gives confidence in the abovementioned transverse-energy values. From the potential at the interstitial site we can draw the conclusion that the incident ion can overcome the interstitial string up to a composition x a little lower than 0.1 and the interstitial plane up to an x value of the order of 0.4 (the temperature correction will increase this value to ~0.45). Therefore, up to these compositions flux peaking near the interstitial atoms must be expected.

Finally we analyzed the flux distribution going from the axial to the planar orientation. Figure 6 shows how the flux is modified as the tilting angle varies keeping concentration constant. In this case the interstitial location is at the center of the channel, so that tilting is along a mixed {110} plane. It can be clearly seen that for intermediate angles (i.e., in the transition region between axial and planar channeling) the flux is no longer uniform near the mixed plane and is more concentrated on the interstitials than on lattice atoms. This means that in the transition region, in which the plane is seen by the incident ion as a discrete structure of strings, [16] the particle can distinguish between stronger and weaker strings and penetrates preferentially into the plane near the latter ones.

B. TiO_x system

In order to establish the validity of a comparison between the SiB_x and TiO_x systems, calculations of continuum potentials for some channels as a function of concentration have also been performed for the latter system.

Figure 7 shows the projection of the hcp crystal lattice of titanium in a perpendicular and parallel direction to the hexagonal [0001] axis (notice that the hexagon shown is not the hexagon of the basal plane). The octahedral interstitial site is denoted by an open circle and the lattice sites by full circles. We remark that the latter lie in two different (0001) planes, denoted by two different symbols (1 and 2); the interstitial plane lies halfway between these planes as is clearly shown in the right side of Fig. 7. The correspondence with Fig. 1 can be easily done: The [0001] axis of titanium corresponds to the [110] axis of silicon (both with the interstitial at the center) and the (0001) plane of titanium, with an interposed oxygen plane, to the (110) plane of silicon with interposed boron planes.

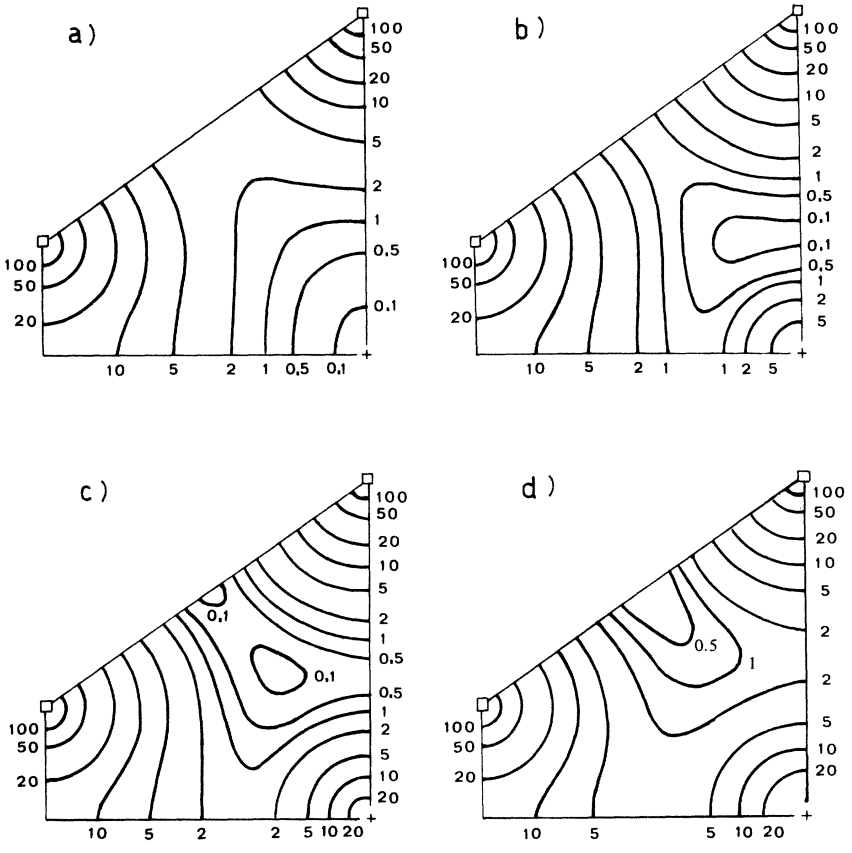

FIG. 4. Equipotential contour plot for standard Lindhard string potential for the same conditions as Figs. 2 and 3. The value at the lattice string is ~130 eV and it depends slightly on impurity concentration.

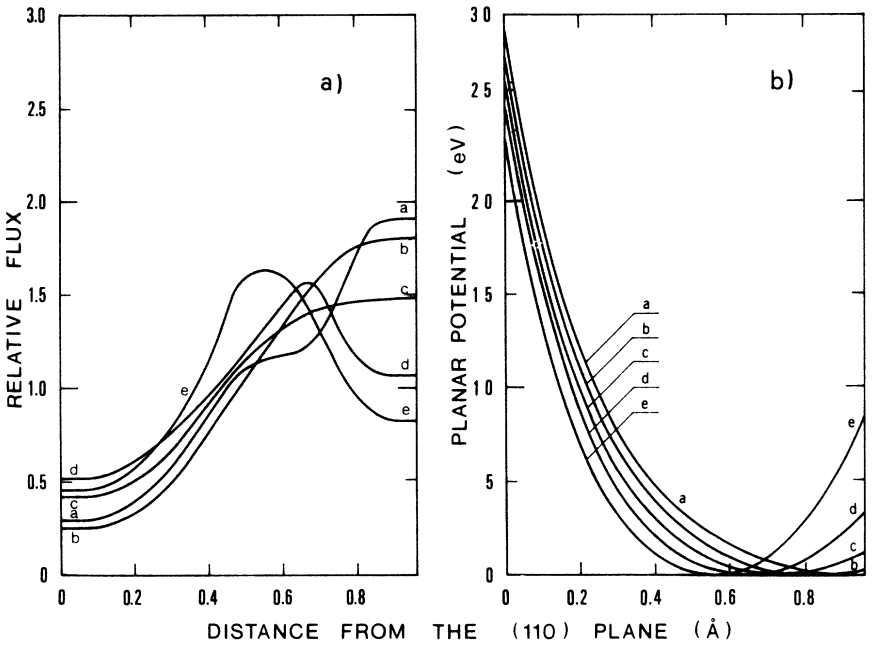

FIG. 5. Particle flux (a) and standard Lindhard planar potential (b) perpendicular to the {110} plane in silicon for different compositions SiB_x. For simplicity the curves are shown only up to half the interplanar distance, where the interstitial plane lies. (a) $x=0$; (b) $x=0.1$; (c) $x=0.25$; (d) $x=0.5$; (e) $x=1$.

Figure 8 shows the continuum potential for the [0001] axial channel as a function of oxygen concentration. The section of the channel drawn in the figure has been chosen for convenience of comparison with the SiB_x system, even though it is excessive as far as only symmetry is concerned. The qualitative behavior is not very different from the silicon case, even though the different symmetry somewhat modifies the results. A more quantitative comparison will be given below.

Figure 9 shows the continuum potential for the (0001) plane. In this case the resemblance with Fig. 5(b) is much greater (except for a scale factor for the ordinates roughly proportional to the ratio of the atomic numbers of Ti and Si).

Table II compares the transverse-energy values with the continuum potential at the interstitial location as a function of concentration both for the axial and planar case. The trend is not very different from the one displayed by silicon in Table I. The only important difference is that in the axial case, for $x=0.1$, the potential at the interstitial string is already somewhat higher than the average transverse energy for the SiB_x system, while this still does not occur in TiO_x. As a consequence a discrepancy between calculations and experiments must be expected at this concentration and the TiO_x system should show a much greater flux peaking at the interstitial site than predicted by calculations on the SiB_x system.

III. EXPERIMENTAL RESULTS

A study of channeling in TiO_x crystals with different oxygen concentrations was performed. 1-MeV deuterons were chosen as projectiles in order to permit simultaneous observations of the channeling behavior both with respect to titanium atoms, by means of wide-angle Rutherford scattering, and to oxygen atoms, by means of the $^{16}O(d, p)^{17}O^*$ reaction. The technical details of the measurements and the procedure of the data analysis were reported in a previous paper.[11] Here we show some significant experimental results to support the theoretical predictions stated above.

Figure 10 shows the composition dependence of the yield of both Rutherford backscattering from the titanium sublattice and of nuclear reaction from oxygen sublattice for ⟨0001⟩ axis. The yields are normalized to the random value. Along the [0001] direction titanium and oxygen atoms lie

TABLE I. String and planar potentials V_{int} at the interstitial position and mean initial transverse energy $\bar{E}_\perp^0$, computed as indicated in the text, for the ⟨110⟩ axis and {110} plane and different compositions in the SiB_x system.

	⟨110⟩ axis		{110} plane	
x	V_{int}(eV)	$\bar{E}_\perp^0$(eV)	V_{int}(eV)	$\bar{E}_\perp^0$(eV)
0.025	1.7	7.2	...	...
0.05	3.8	7.0	...	...
0.1	8.3	6.7	0.3	2.8
0.25	22.3	6.6	1.2	2.4
0.5	46.8	7.7	3.3	2.3
1	...	...	8.2	2.7

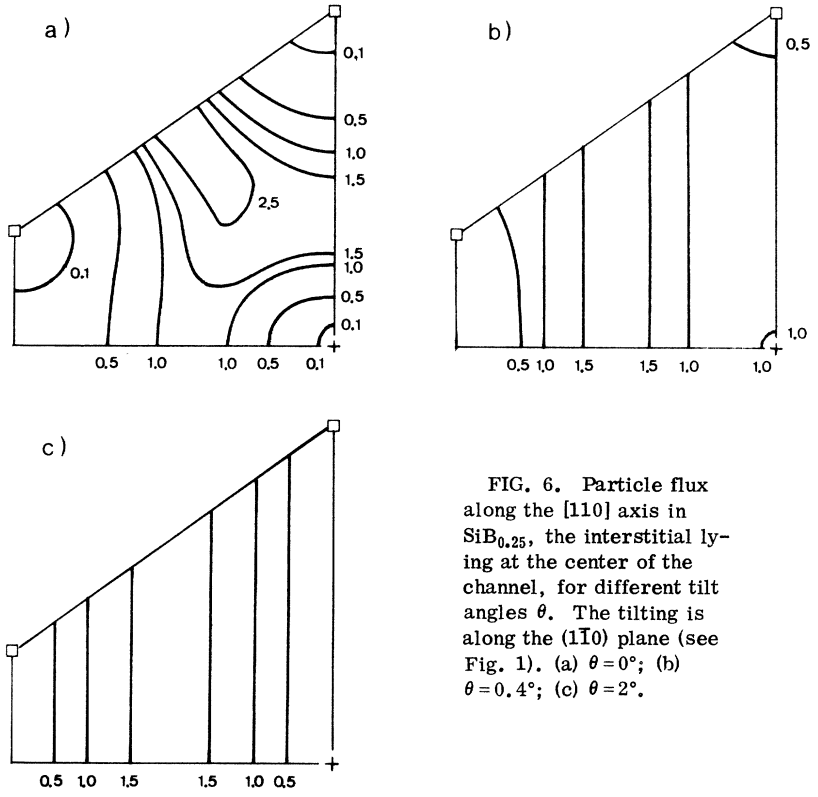

FIG. 6. Particle flux along the [110] axis in $SiB_{0.25}$, the interstitial lying at the center of the channel, for different tilt angles θ. The tilting is along the $(1\bar{1}0)$ plane (see Fig. 1). (a) $\theta = 0°$; (b) $\theta = 0.4°$; (c) $\theta = 2°$.

on separate rows. The tilt angle was within the $\{1\bar{2}10\}$ plane, which contains both titanium and oxygen atoms (mixed plane, see Fig. 7). At low concentrations ($x = 0.1$) the oxygen sublattice does not yet give rise to channeling effects and we observe flux peaking at the oxygen string. Notice that the term flux peaking is somewhat inadequate to describe the real situation at this concentration because the peak yield at the oxygen site is nearly equal to the random yield; this is due to the balanced repulsive effect of titanium and oxygen strings on the incident ion. At higher concentrations ($x = 0.2$) the oxygen string is strong enough to display a yield dip in the nuclear reaction. Of course the different strengths of titanium and oxygen strings are reflected in the different values of the dips. We recall that similar results have been obtained for the $\langle 1\bar{2}10 \rangle$ axis but, owing to the completely different symmetry of the channel, no computer simulation was made.[11] Another interesting feature is shown in Figs. 10(c) and 10(d). We see that when the crystal is tilted around the axis along the crystal plane, the oxygen sublattice gives rise to much higher shoulders than the titanium, arriving up to approximately the random yield. This symmetry in the yield at the axial-to-planar channeling transition is also predicted by computer simulations (see Fig. 6).

Figure 11 shows the normalized yield for the (0001) plane at various compositions: As shown in Fig. 7, the (0001) planes consist of a single atomic species. The scattering curves relative to the titanium sublattice always show the expected channeling effect, while the nuclear-reaction yield from the oxygen sublattice always gives a peak higher than the random value for planar alignment. The steering power of the pure-oxygen planes appears to be too weak to maintain a steered trajectory. The oxygen planes may still be considered as made of single interstitial atoms randomly arranged and

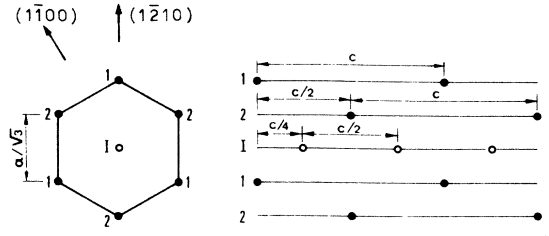

FIG. 7. Front and side view of the [0001] channel in titanium. a and c denote the lattice constants. The symbols I, 1, and 2 and the open and full circles have the same meaning as in Fig. 1.

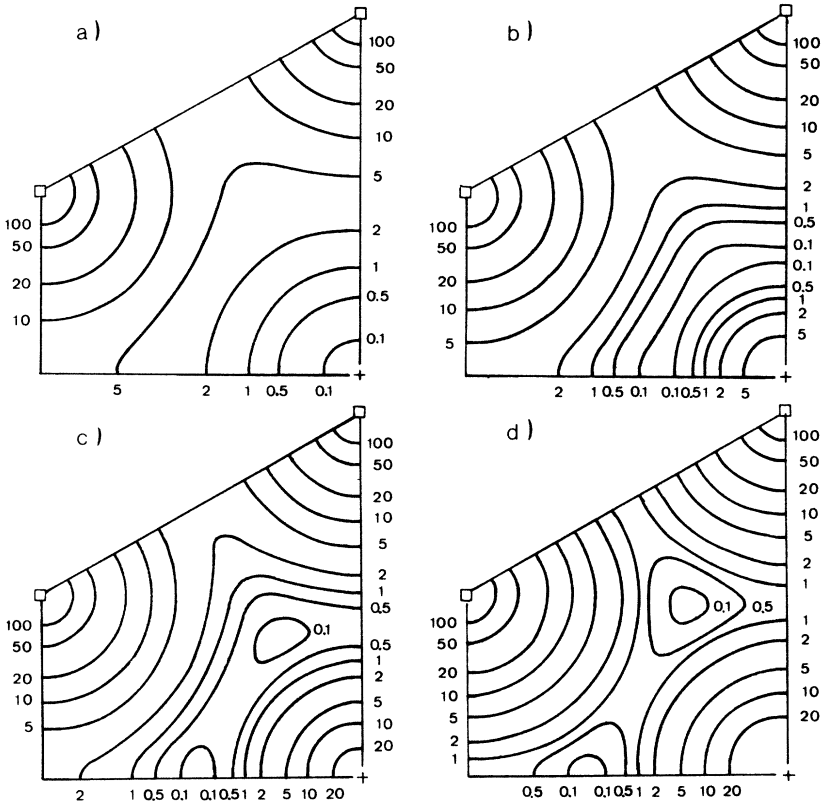

FIG. 8. Equipotential-contour plot for standard Lindhard string potential for deuterons along the [0001] axis in titanium containing oxygen atoms at the center of the channel for different TiO_x compositions. The value at the lattice string is ~115 eV and it depends slightly on impurity concentration. □, Ti site; +, O site (only a quarter of the channel is shown for an easier comparison with Fig. 4). (a) $x=0$; (b) $x=0.1$; (c) $x=0.25$; (d) $x=0.5$.

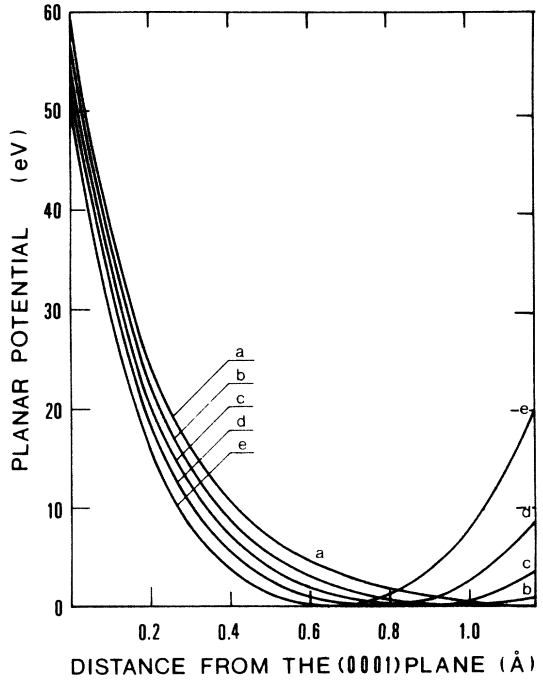

FIG. 9. Standard Lindhard planar potential perpendicular to the (0001) plane in titanium for different TiO_x compositions. As in Fig. 5 the curves are shown only up to the interstitial plane. (a) $x=0$; (b) $x=0.1$; (c) $x=0.25$; (d) $x=0.5$; (e) $x=1$.

the flux peaking at half the distance between pure titanium planes is maintained up to the highest oxygen concentration investigated ($x=0.39$). However, the experiments also show that planar flux peaking is progressively destroyed at the interstitial site with increasing interstitial concentration. Similar results have been obtained for the $\{10\bar{1}0\}$ planar configuration (see Fig. 7).[11]

Table III compares the experimental results with computer simulations, both for interstitial and lattice atoms. The small differences with Table VIII of Ref. 11 are due to a better statistics. Computer values are given for two different grid squares, of sides approximately equal to a_{TF} and $2a_{TF}$, respectively. The values are computed at a

TABLE II. Same as Table I but for the [0001] axis and (0001) plane and different compositions in TiO_x system.

	[0001] axis		(0001) plane	
x	V_{int}(eV)	$\bar{E}_1^0$(eV)	V_{int}(eV)	$\bar{E}_1^0$(eV)
0.025	1.0	9.4	...	...
0.05	2.8	9.0	...	...
0.1	6.7	8.5	0.9	5.5
0.25	19.2	8.0	3.5	5.0
0.5	41.2	8.2	8.7	5.1
1	...	...	20.4	6.4

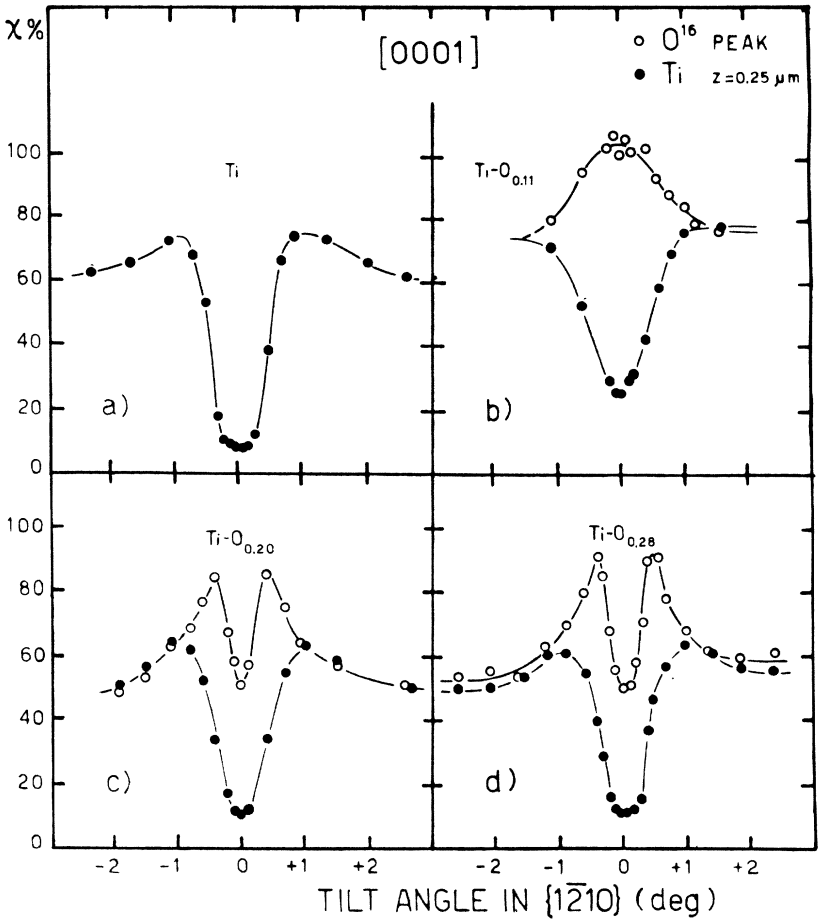

FIG. 10. Channeling normalized yields for the [0001] axis at various TiO_x compositions. Tilt angle is within a {1$\bar{2}$10} plane (see Fig. 7). Open circles denote proton yield from nuclear reaction and full circles deuteron backscattering yield from titanium atoms. The results refer to a depth of about 3000 Å below the surface. (a) $x=0$; (b) $x=0.11$; (c) $x=0.20$; (d) $x=0.28$.

TABLE III. Computed flux for 1-MeV deuterons at 3000 Å below the surface in the SiB_x system compared with the experimental yield in the TiO_x system. The values of composition x referring to calculations and experiments are denoted with x_{calc} and x_{expt}, respectively; the difference between the two arises from the fact that in our computer model the composition could be varied only by discrete steps. The approximate side of the grid squares used to compute the flux are denoted by a_{TF} and $2a_{TF}$. *C* and *S* refer to the boron interstitial location, meaning "Center" and "Side" of the axial channel, respectively. The tilting angles for the *C* location are measured relative to either the [110] or [0001] axis and within either the (1$\bar{1}$0) or (1$\bar{2}$10) plane for SiB_x and TiO_x, respectively. The tilting angle of 2° for the *S* location refers only to computed values and is measured from the [1$\bar{1}$0] axis within the (110) plane, corresponding to planar channeling; the experimental data refer to the (0001) planar alignment.

Tilting angle	Atomic concentration x_{calc}	Atomic concentration x_{expt}	Interstitial location	Normalized flux at interstitial site $\sim a_{TF}$	Normalized flux at interstitial site $\sim 2a_{TF}$	Normalized flux at interstitial site Experimental yield	Normalized flux at lattice site $\sim a_{TF}$	Normalized flux at lattice site $\sim 2a_{TF}$	Normalized flux at lattice site Experimental yield
0°	0.10	0.11	*C*	0.35	0.85	1.00	0.03	0.07	0.25
2°	0.10	0.11	*C*	0.35	0.45	0.75	0.35	0.45	0.75
0°	0.25	0.28	*C*	0.10	0.35	0.50	0.07	0.10	0.10
0.4°	0.25	0.28	*C*	1.05	0.85	0.90	0.25	0.50	0.40
1°	0.25	0.28	*C*	0.45	0.50	0.70	0.55	0.60	0.65
2°	0.25	0.28	*C*	0.20	0.40	0.55	0.20	0.40	0.55
2°	0.10	0.11	*S*	1.80	1.65	1.30	0.25	0.35	0.45
2°	0.25	0.28	*S*	1.45	1.45	1.20	0.45	0.55	0.60
2°	0.50	0.39	*S*	1.05	1.30	1.15	0.50	0.65	0.60

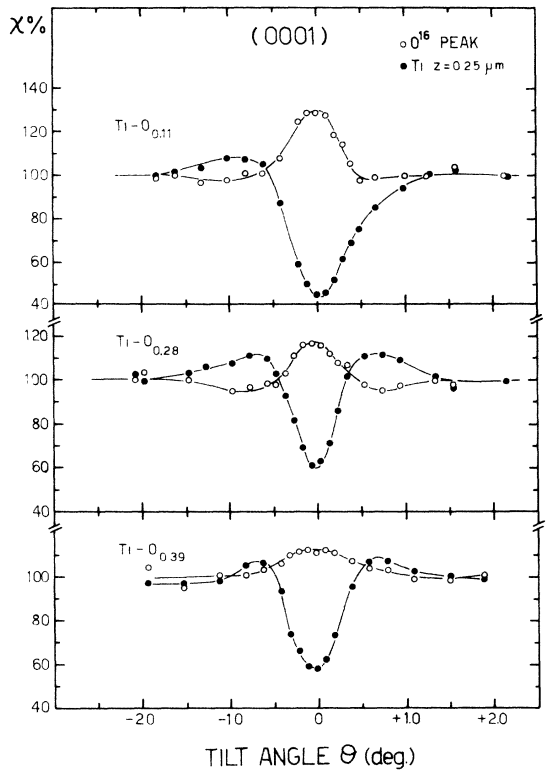

FIG. 11. Channeling normalized yield for the (0001) plane at various TiO_x compositions. The depth is the same and the open and full circles have the same meaning as in Fig. 10. (a) $x=0.11$; (b) $x=0.28$; (c) $x=0.39$.

depth of 0.3 μm. We did not take into account possible differences in depth scale, due to the different stopping powers of deuterons in silicon and titanium, since the flux averaged over the well known depth oscillations does not show any variation from 0.2 to 0.4 μm, so that the chosen value for the depth is not very critical. The agreement turns out to be better with values computed with the largest grid squares. This can be due partly to better statistics and partly to the limitations of our computer model, which seems to underestimate the "nuclear encounter probability" (see the second paper of Ref. 12). However, the general trend is also displayed by the smaller grid. The only serious discrepancy occurs for axial channeling at $x=0.1$, where flux peaking at the interstitial site is definitely underestimated by computations. This discrepancy was expected, however, on the basis of the differences between the two lattices (see the end of Sec. IIB).

IV. CONCLUSIONS

The main results obtained in the present work may by summarized as follows.

(i) The agreement between experiments and computer simulations ensures the general validity of our results, at least in the case of $Z_{\text{lattice}}/Z_{\text{interstitial}} \simeq 2.8$ and a quasihexagonal symmetry. Of course the exact composition values at which interstitial strings and planes become effective will depend upon the precise nature of the system.

(ii) In the axial case for low concentrations ($x=0.1$) we have a maximum flux at the interstitial site of the order of the random value, while for higher concentrations ($x=0.2$) a yield dip occurs.

(iii) On the contrary in the planar case the dip does not appear up to a composition $x \simeq 0.5$ and the ion flux at the interstitial site remains higher than the random, while decreasing with increasing impurity concentration.

(iv) The effectiveness of the interstitial string or plane on the incident-particle path cannot be simply estimated by neglecting the simultaneous effect of the host lattice, as we did in our previous paper.[11] The resulting effects are determined by a relative balancing between the transverse energy acquired when the ion enters into the crystal and due essentially to the host lattice and the height of the barrier due to the interstitial array.

(v) At the axial-to-planar channeling transition the ion does not see a continuous plane any longer but distinguishes between stronger and weaker strings and penetrates preferentially near the latter ones giving rise to a much higher shoulder in the yield of the process at the interstitial than at the lattice site, which in our case turns out to be of the order of the random value.

In conclusion, the agreement between experiments and computer simulations show the rather general value of our results with respect to the role of an interstitial sublattice. In particular, in the interpretation of experiments the reciprocal interaction of the various types of strings and planes must be taken into account, as suggested by other authors (see the second of Ref. 7). The importance of systematic investigations of this kind for problems such as atom location is also evident, because interstitial string effects can arise with increasing concentration, especially with impurities of high atomic number.

---

*Experimental work performed at Laboratori Nazionali di Legnaro, Italy. Research sponsored in part by Gruppo Nazionale di Struttura della Materia del Consiglio Nazionale delle Ricerche.

†On leave from the Research Institute for Iron, Steel and Other Metals, Tohoku University, Sendai, Japan.

‡Istituto Chimico, Facoltà di Ingegneria, Università di Bologna, Bologna, Italy.

[1]R. B. Alexander, G. Dearnaley, D. V. Morgan, J. M. Poate, and D. Van Vliet, in *Proceedings European Conference on Ion Implantation* (*Reading*, 1970) (Peter Peregrinus, Stevenage, 1970), p. 181; D. Van Vliet, Radiat. Eff. 10, 137 (1971).

[2]J. H. Barrett, Phys. Rev. B 3, 1527 (1971).

[3]H. D. Carstanjen and R. Sizmann, Radiat. Eff. 12, 225 (1972).

[4]M. A. Kumakhov, Phys. Lett. A 32, 538 (1970); Radiat. Eff. 15, 85 (1972).

[5]J. U. Andersen, O. Andreasen, J. A. Davies, and E. Uggerhøj, Radiat. Eff. 7, 25 (1971).

[6]R. B. Alexander, P. T. Callaghan, and J. M. Poate, Phys. Rev. B 9, 3022 (1974).

[7]D. S. Gemmell and R. C. Mikkelson, Radiat. Eff. 12, 21 (1972); Phys. Rev. B 6, 1613 (1972).

[8]F. Abel, G. Amsel, M. Bruneaux, and C. Cohen, Radiat. Eff. 12, 35 (1972).

[9]R. Hellborg, Phys. Scr. 3, 279 (1971); 4, 203 (1972).

[10]L. Eriksson and J. A. Davies, Ark. Fys. 39, 439 (1969).

[11]G. Della Mea, A. V. Drigo, S. Lo Russo, P. Mazzoldi, S. Yamaguchi, G. G. Bentini, A. Desalvo, and R. Rosa, in Proceedings of the Fifth International Conference on Atomic Collisions in Solids, Gatlinburg, 1973 (unpublished).

[12]A. Desalvo, R. Rosa, and F. Zignani, J. Appl. Phys. 43, 3755 (1972); G. Della Mea, A. V. Drigo, S. Lo Russo, P. Mazzoldi, G. G. Bentini, A. Desalvo, and R. Rosa, Phys. Rev. B 7, 4029 (1973).

[13]W. A. Harrison, *Solid State Theory* (McGraw-Hill, New York, 1970), p. 381.

[14]G. Foti, F. Grasso, R. Quattrocchi, and E. Rimini, Phys. Rev. B 3, 2169 (1971).

[15]B. R. Appleton, C. Erginsoy, and W. M. Gibson, Phys. Rev. 161, 330 (1967).

[16]A. Desalvo and R. Rosa, Phys. Rev. B 9, 4605 (1974).

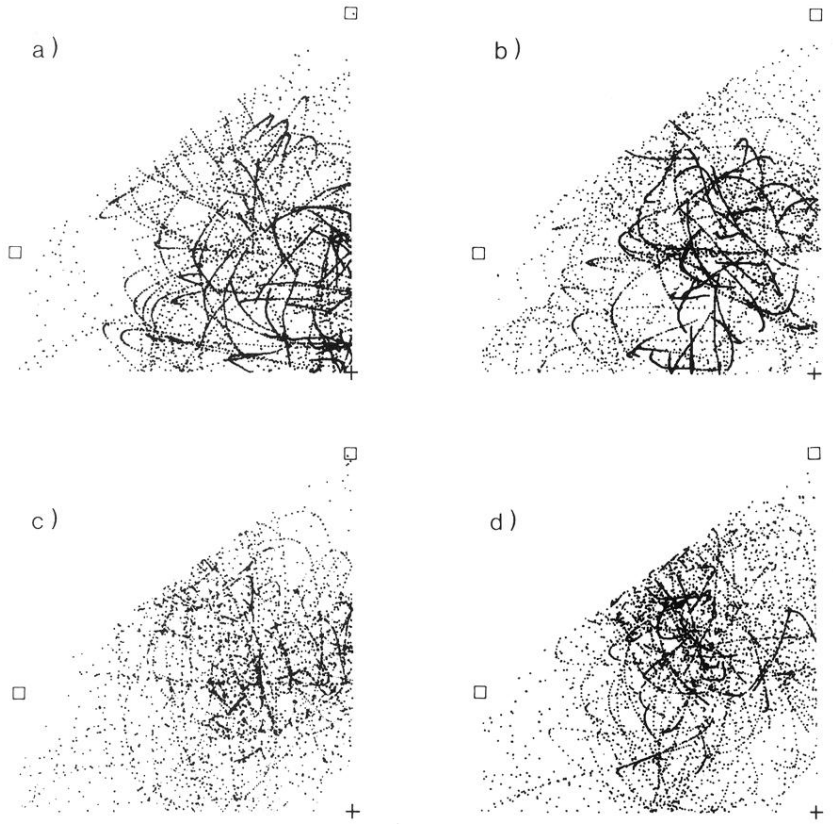

FIG. 2. Dot-density plot of 100 trajectories of 1-MeV deuterons incident parallel to the ⟨110⟩ axis in silicon containing boron atoms at the midchannel axis, for different compositions SiB_x. The paths are plotted from 2400 to 3000 Å below the surface; for clarity only one point each three steps of the ion path is plotted. □, Si site; +, B site (only one quarter of the channel is shown). (a) $x = 0$; (b) $x = 0.1$; (c) $x = 0.25$; (d) $x = 0.5$.